Available online at www.sciencedirect.com
SCIENCE DIRECT®
International Journal of Heat and Mass Transfer 49 (2006) 4584–4595
International Journal of HEAT and MASS TRANSFER
www.elsevier.com/locate/ijhmt

Comprehensive optimization of a heat pipe radiator assembly filled with ammonia or acetone

Valeri V. Vlassov *, Fabiano L. de Sousa, Walter K. Takahashi

National Institute for Space Research (INPE/DMC), Av. dos Astronautas, 1758. S.J.Campos, SP, 12227-010, Brazil

Received 2 November 2005
Available online 10 July 2006

Abstract

Optimal mass characteristics for a heat pipe radiator assembly for space application are investigated. The assembly consists of the heat pipe itself, an evaporator saddle and a radiator. The internal HP geometry and the dimensions of the saddle and radiator panel are the variables to be optimized. Operational and structural constraints are considered and the assembly is optimized for different operational modes in 0*g* and 1*g* gravity conditions. A new global search metaheuristic, called generalized extremal optimization, was used as the optimization tool. The results show that under certain combinations of input parameters the assembly with acetone HP can be more weight effective than the one with ammonia, in spite of the liquid transport factor criterion indicates an opposite trend.

Keywords: Grooved heat pipe; Radiator assembly; Optimal design; Stochastic optimization

1. Introduction

Heat pipes have been applied in thermal control systems of satellites and spacecraft for many years. It is a very appropriate device for space applications: it does not need electric power, has no moving parts, has a very effective thermal conductance and has a long operational life.

Typically, the heat pipe (HP) consists of a hermetically sealed tube-type container, having a porous structure fixed to its internal wall. The HP is filled with a small amount of a working fluid by such a way that liquid completely soaks into the wick, whereas vapor occupies the central core. After applying heat on one end of the HP, the liquid evaporates, flows to the colder end and condenses there. Under capillary action liquid returns through the wick to the evaporation section, closing the heat and mass transfer cycle. Due to the high value of the latent heat of the fluid, the mass flow rate, needed to transport the heat to a specified distance, is small enough to be pumped only by capillary tension forces at 0-gravity (0*g*) conditions.

There are two main kinds of HP applications in satellites: (i) for transferring heat to a radiator over large distances from areas where there are equipment with high heat dissipation or; (ii) for spreading heat over a structural panel to minimize thermal gradients over it. In this paper we will focus on the first kind of application. A typical HP radiator assembly (HPRA) for transferring heat consists of a HP coupled, at one end, to a space radiator, while its other end is connected to a saddle to provide mechanical and thermal interface to the equipment. In Fig. 1 is depicted such an arrangement.

For HP assemblies, a typical design procedure usually consists of three practically independent stages: (i) first, the most effective working fluid is selected for the desired operational temperature range, then; (ii) a type of HP of minimal mass is selected that, when filled with the chosen fluid, is capable of transferring the specified heat flux under worst hot conditions and, finally; (iii) a saddle and radiator sized to meet thermal and strength requirements, is added.

Many studies were done on working fluids for space application HPs in the early 1970s. These studies showed that ammonia was the best candidate. In spite of being a hazardous, toxic and high-pressure working fluid, it has

* Corresponding author.
E-mail address: vlassov@dem.inpe.br (V.V. Vlassov).

0017-9310/$ - see front matter © 2006 Elsevier Ltd. All rights reserved.
doi:10.1016/j.ijheatmasstransfer.2006.02.059

Nomenclature

A	area, m
B	width, m
b	width, m
Bo	bond number
C_p	sensible heat, J/kg/K
D	diameter, m
E	Young modulus, Pa
F	force, N
$\hat{f}$	force per length, N/m
g	gravity acceleration, m/s^2
h	effective height, m, or heat transfer coefficient, W/K/m^2
I	moment of inertia, m^4
K	permeability, m^2
k	thermal conductivity, W/m/K
L	length, m
M	mass, kg
$\hat{M}$	mechanical moment, N m
$\dot{m}$	mass flow rate, kg/s
n	gravity overload
Q	heat rate, W
q	heat flux , W/m^2
T	temperature, K
u	yield strength, Pa
w	width, m
y	deflection, m

Greek symbols

α	absorptivity
β	design safety factor
γ_v	adiabatic constant
δ	thickness, m
δ'	tilt, m
ε	effective porosity, or emissivity
η	effectiveness
μ	dynamic viscosity, Pa s
ρ	Density, kg/m^3
σ	Stefan–Boltzmann constant, W/m^2/K^4
σ'	surface tension, N/m
$\hat{\sigma}$	stress, Pa
θ	wetting angle
λ	latent heat, J/kg
φ	angle for artery

Subscripts

a	adiabatic
ar	artery
A	albedo
BOL	begin-of-life
c	condenser
e	evaporator
eff	effective
EOL	end-of-life
eq	equipment
ext	external
f	fluid
g	gravity
h	hydraulic
hp	heat pipe
IR	infra-red
l	liquid
p	porous
r	radiator
t	tilt
tst	ground testing
tvc	shroud of vacuum chamber
v	vapor
w	wall
$\sum$	total

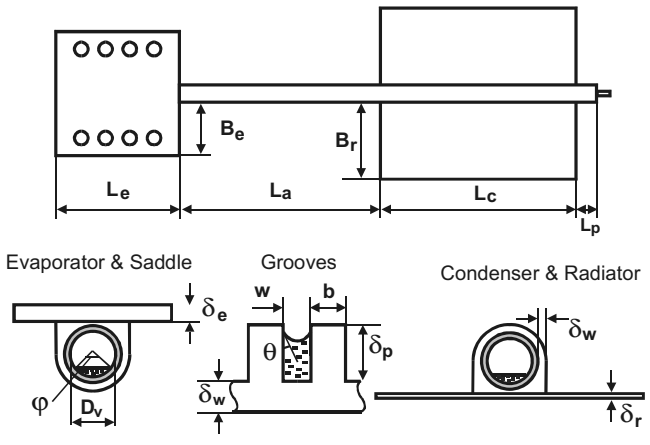

Fig. 1. HP assembling geometric parameters.

the best value of liquid transport factor (LTF), defined in [1] and [8] as $N_l = \sigma\lambda\rho\mu^{-1}$, for the operation temperature range of electronic equipment (~−10 to +45 °C). It is also compatible with light-weight aluminum alloys. Even though other fluids are compatible with aluminum, they practically are not considered as competitive candidates due to inferior liquid transport factor.

In space applications, mass optimization is a mandatory aspect of the design process. Hence, a HP assembly should have the least possible mass. Although the HP itself is usually a light-weight unit, the masses of the saddle and radiator may have significant figures. Moreover, the key dimensions of these three units are related to each other. For example, in attempting to minimize the weight of the assembly, one can wish to select a HP with a minimal diameter. However, this would lead to a decrease in the area of contact between the HP tube and the radiator

and consequently in an increase of the thermal gradient along the radiator width (see Fig. 1), reducing its thermal efficiency. This area, where the HP is attached to the radiator, provides near-isothermal conditions; from this point of view, the higher the HP diameter, the higher radiator overall effectiveness, and therefore it could has a smaller area and, consequently, mass for given heat rate. A similar rationale is applicable to the saddle as well. A long-length radiator is more effective than, say, a square-shaped one (keeping the same area of radiation), however the former design causes the HP length (and mass) to increase. A shorter saddle certainly has a lesser mass, however reducing the evaporation area can cause violation of the HP boiling limit, especially for one with a small diameter. A HP that uses a working fluid with high saturation pressure, such as ammonia, must have a thicker wall to meet safety requirements, causing additional unit mass. In fact, the choice of the design parameters of a HPRA are also dependent on the strength constraints and the mechanical loads applied to the assembly.

As far as we know, there are no publications on the optimization of the HP parameters at the assembly level, with consideration of thermal and mechanical constraints simultaneously. In this work we perform a comparison of the minimal mass characteristics of two HP assemblies, one filled with ammonia and another with acetone. Both designs are optimized by the proper selection of design parameter values to minimize the assembly mass, at the same operational condition.

Another important aspect of HPs designed to space applications, is that they must work under very different ambient conditions. At least two extreme orbital cases must be considered: extreme cold and hot operational conditions. Usually, the cold condition corresponds to longer eclipse orbits, low solar intensity and minimal heat dissipation of equipment, whereas the hot condition corresponds to shorter eclipses and maximum heat dissipation of equipment. Moreover, although the HP is designed to operate at $0g$ conditions, it must be tested at ground conditions ($1g$) during its development, qualification, integration and acceptance tests.

The variety of operational conditions that the HP is exposed to causes an additional problem: the existence of excess of liquid in the vapor channel. The excess of liquid occurs due to the recession of the meniscus under normal operation and also because of the thermal expansion of liquid under operation at hot conditions. This excess of liquid forms a liquid slug, which in $0g$ conditions partially blocks the condenser from the cold end, reducing the effective temperature of the attached radiator. During ground tests in which the HP is on horizontal position, differently from the $0g$ case, the excess of liquid usually forms a puddle, which acts as an eventually artery along the entire HP length. This artery contributes on supplying liquid to the evaporator section, improves the integral hydraulic characteristics of the liquid channel and therefore the capillary limit. Besides, as is shown in [22], the puddle reduces the effective HP elevation. However, if the diameter of the HP vapor channel is small, such that the Bond number is less than 1, the slug may be formed at $1g$ as well. A detailed theoretical and experimental study for the conditions under which a slug forms at the end of the vapor space was carried out by Eninger and Edwards in 1977 [21].

This excess of liquid causes alterations on the HP characteristics and must be taken into account in the design procedure. It is noteworthy that a especially dedicated flight experiment (Shlitt [2], in 1986) was entirely devoted to the investigation of how the slug of liquid excess can affect the performance of a HP at $0g$ with comparison to ground conditions. In this experiment, the slug occupied from 5.4% to 8.2% of the HP length from the condenser end.

As far as we know, there are no publications on the subject of HP design optimization, considering all operational and test conditions simultaneously and the related problem of excess liquid. The usual less complicated approach was to tackle only the worst hot $0g$ case [20,3,4]. However under certain circumstances, the cold condition may cause the capillary limit to be violated, for instance, because of the increase of the liquid viscosity or reduction of vapor density. Thus, the consideration of all operational conditions simultaneously is essential.

To perform the numerical optimization of a HP, it is necessary to have a proper mathematical model that simulates its thermohydraulic features, as well as an optimization algorithm capable of tackling complex design spaces. The mathematical modeling of heat and hydraulic interlinked processes inside a HP presents a complicated issue. Most of the research is devoted to the mathematical modeling of local processes, particularly to the evaporation–condensation in the porous structure and in micro-grooved channels, or on 2D vapor flow simulations inside the HP core. Although some complex steady state and transient mathematical models have been developed [5–7], reduced engineering HP models, developed in the 1970s [1,8] continue to be used for design purposes. These models, in spite of being simplified, fit well with experimental data, particularly for axially-grooved HPs, due to its well-determined geometry [9,7]. Such models yield effective numerical procedures and can be combined efficiently with stochastic optimization algorithms.

The heat pipe comprehensive optimization problem is considered unsuitable for traditional gradient-based methods [3]. In fact, it is a complex nonlinear problem with implicit design variables and subject to many nonlinear constraints; therefore it is prone to have a design space with many sub-optimal solutions. In this type of space, a global search algorithm would have a better chance to find the global optimum. In a previous work [10] the first and second authors used a new global search meta-heuristic, called generalized extremal optimization (GEO), to optimize a single unit – mesh type heat pipe, and the same method is used here to the optimization of the radiator assembly with axially-grooved HP.

Summarizing, in this work we present a new approach to the design of a HPRA for a space application. The main distinctions from the traditional way of optimal designing this kind of system are (1) different operational conditions, which includes flight hot, cold and ground test ones, are incorporated simultaneously to the optimization problem; (2) the optimization is done at assembly level, that is, taking into account simultaneously the HP, radiator and saddle and; (3) typical stress loads acting over the HPRA during launch to orbit are also taken into account during the optimization process. The mathematical model of the HP is based on the well known and proved simplified HP models [7,8,11], however we modified them by including procedures to address excess of liquid at $0g$ and $1g$ conditions. This approach is used here to optimize a HPRA with a grooved type HP, for two working fluids: ammonia and acetone. The GEO algorithm is used as the optimization tool.

2. General statement of the optimization problem

The optimization criterion is to minimize the total design mass of the HP radiator assembly, for a specified heat transferring capability, over a given distance, under different operational conditions. All HPRA basic dimensions are taken as design variables, forming the vector $\bar{x}$ to be optimized.

The other parameters of the problem are separated in distinct vector groups, as follows: $\bar{s}$ – vector of mode-independent fixed input parameters (mechanical properties, adiabatic length, etc.); $\bar{p}_k$ – vectors of mode-dependent fixed input parameters for each kth operational mode; $\bar{y}_k$ – vectors of mode-dependent regime parameters (temperatures, pressures, mass flow rates, etc.), whose values are coming from the HPRA numerical model; $\bar{y}_0$ – vector of parameters, depended of all operational modes (liquid excess slug and artery parameters); $\bar{r}_k$ – vectors of physical properties of fluid at current saturation conditions.

The optimization problem is stated as a mathematical programming problem having sets of inequality and bound constraints, and can be mathematically stated as

Objective function: $\min_{\bar{x}} M_{\Sigma}(\bar{x}, \bar{s}, \bar{y}_o)$.

Constraints:

$$R_{0g}: \begin{cases} \underset{k\in R_{0g}}{\text{Operational mode } k:} \begin{cases} f_1(\bar{x},\bar{s},\bar{p}_k,\bar{r}_k,\bar{y}_k) \otimes 1 \\ \cdots\cdots \\ f_m(\bar{x},\bar{s},\bar{p}_k,\bar{r}_k,\bar{y}_k) \otimes 1 \end{cases} \end{cases}$$

$$R_{1g}: \begin{cases} \underset{k\in R_{1g}}{\text{Operational mode } k:} \begin{cases} f_1(\bar{x},\bar{s},\bar{p}_k,\bar{r}_k,\bar{y}_k) \otimes 1 \\ \cdots\cdots \\ f_m(\bar{x},\bar{s},\bar{p}_k,\bar{r}_k,\bar{y}_k) \otimes 1 \end{cases} \end{cases}$$

$$R_x: \begin{cases} \text{All modes}: \begin{cases} \varphi_{mk+1}(\bar{x},\bar{s}) \otimes 1 \\ \cdots\cdots \\ \varphi_{mk+M}(\bar{x},\bar{s}) \otimes 1 \end{cases} \\ \text{Side bounds}: \{x_i^- \leqslant x_i \leqslant x_i^+, \quad i = 1,\ldots,n \end{cases}$$

HP radiator assembly model:

$$\begin{cases} \bar{y}_k = \Phi(\bar{x},\bar{s},\bar{p}_k,\bar{r}_k,\bar{y}_k), & k \in R_{0g} \\ \bar{y}_k = \tilde{\Phi}(\bar{x},\bar{s},\bar{p}_k,\bar{r}_k,\bar{y}_k), & k \in R_{1g} \\ \bar{y}_0 = \Psi(\bar{x},\bar{s},\bar{y}_1,\bar{y}_2,\ldots,\bar{y}_k,\ldots,\bar{y}_N). \end{cases}$$

In the general statement of the problem given above, the following notation was adopted: symbol $\otimes$ means either $\leqslant$ or $\geqslant$; m – the number of constraints related to operational modes; $N_{0g} - N_{1g}$ – number of weightless and gravity operational modes, respectively; $\Phi(\bar{x},\bar{p}_k)$ – either a system of equations, an algorithm, or numerical procedure, which calculates all regime parameters for all operational modes at $0g$ or $1g$ $\left(\tilde{\Phi}(\bar{x},\bar{p}_k)\right)$ conditions; $\phi_j(\cdot)$ – mode-independent constraints (usually, strength relationships); x_i^-, x_i^+ – lower and upper bounds of the design variables.

All constraints are separated in three groups: R_x – all-modes or mode-independent constraints; R_{0g} – constraints for the modes of weightless (flight) conditions; R_{1g} – constraints for the modes of (ground) test conditions.

3. Operational modes, fixed parameters and optimized variables

The optimal design problem states that the total mass of the assembly must be as minimal as possible, under the condition that the device should transfer a determined heat rate through a defined distance of adiabatic section (L_a), for all operational conditions and at both $1g$ and $0g$ environments. The design variables are the length of evaporator and condenser sections, the width and thickness of saddle and radiator, the diameter of the vapor core, the HP thickness and the internal parameters of the grooves. The vector of design variables to be optimized is composed of 11 parameters: $\bar{x} = \{D_v, L_e, L_c, B_e, B_r, \delta_e, \delta_r, \delta_w, \delta_p, b, w\}$.

Any combination of a specified heat transport capability (Q_i) with a determined environmental condition is considered an operational mode. A set of mode-dependent fixed parameters $\bar{p}_k$, defines an operational mode. The modes considered in this work are summarized in Table 1. The modes 1, 3, 5 are considered as principal ones for specified heat load Q_{max}, whilst other modes are included in the model for extended studies.

The temperature limits for the equipment that would be attached to the saddle ($T_{eq,min}$ and $T_{eq,max}$) are also components of the input vector $\bar{p}_k$ and in generally they are different for each operational mode. Hence $\bar{p}_k = \{Q_{x,k}, q_{ext,k}, T_{rvc,k}, \delta'_{t,k}, T_{eq\,max,k}, T_{eq\,min,k}\}$. Other input parameters are mode-independent. They compose the vector $\bar{s}$ and are shown in Table 2.

The thermo-physical properties of the HP working fluid at saturation conditions are also fixed parameters. In the statement of the optimization problem they compose the vector $\bar{r}_k$, $\bar{r}_k = \{P_{s,k}, \lambda_k, \sigma_k, C_{pl,k}, \mu_{l,k}, \rho_{l,k}, C_{pv,k}, \mu_{v,k}, \rho_{v,k}\}$. The properties are dependent of saturation temperature, which is calculated by the HPRA model from saturation property tables [12] by interpolation.

Table 1
Operational modes and mode-dependent fixed parameters

	Mode: k	Mode description	Fixed parameters: components of $\bar{p}_k$			
			$Q_{x,k}$ [W] heat load	$q_{\text{ext},k}$ [W/m^2] (external heat flux at 0g)	$T_{\text{rvc},k}$ [K] (temp of shroud of vacuum chamber)	$\delta_{\text{t},k}$ [m] tilt at 1g
R_{0g}	1	0g operational "hot"	$Q_{x1} = Q_{\max}$	$q_{\text{ext1}} = q_{\max}$	–	$\delta_{\text{t1}} = 0$
	2	0g operational (stand-by)	$Q_{x2} = Q_{\min}$	$q_{\text{ext2}} = q_{\max}$	–	$\delta_{\text{t2}} = 0$
	3	0g operational	$Q_{x3} = Q_{\max}$	$q_{\text{ext3}} = q_{\min}$	–	$\delta_{\text{t3}} = 0$
	4	0g operational (stand-by) "cold"	$Q_{x4} = Q_{\min}$	$q_{\text{ext4}} = q_{\min}$	–	$\delta_{\text{t4}} = 0$
R_{1g}	5	1g testing, horizontal, "hot"	$Q_{x5} = Q_{\text{tst1}}$	$q_{\text{ext5}} = 0$	$T_{\text{rvc5}} = T_{\text{tst1}}$	$\delta_{\text{t5}} = \delta_{\text{t}}$
	6	1g testing, horizontal, "cold"	$Q_{x6} = Q_{\text{tst2}}$	$q_{\text{ext6}} = 0$	$T_{\text{rvc6}} = T_{\text{tst2}}$	$\delta_{\text{t6}} = \delta_{\text{t}}$

Table 2
Values of mode-independent fixed parameters ($\bar{s}$)

No.	Symbol	Description	Unit	Value
1	ε_{r}	Emissivity of radiator (White paint S13)	–	0.88
2	α_{BOL}	Absorptivity of radiator (White paint S13, BOL)	–	0.21
3	α_{EOL}	Absorptivity of radiator (White paint S13, EOL)	–	0.56
4	g_{eq}	Specific thermal conductance at equipment interface	W/K/m^2	700
5	$\theta_{\min}$	Wetting angle of HP grooves	deg	5
6	r_{n}	Nucleate radius in HP grooves	m	2.5×10^{-7}
7	$T_{\max}$	Maximum non-operating temperature	°C	85
8	L_{a}	Length of adiabatic section	m	0.4
9	β	Safety strength factor	–	4 or 2.5
10	$\dot{\omega}$	Max angular velocity of satellite during attitude control system action	1/s	$2\pi/1800$
11	$\ddot{\omega}$	Max angular acceleration of satellite during attitude control system action	1/s^2	$2\pi/900^2$
12	$\{u_{\text{e}}; u_{\text{c}}; u_{\text{w}}\}$	Properties of Al alloy: ultimate stress limit, thermal conductivity and density	MPa	192
13	$\{k_{\text{w}}, k_{\text{p}}\}$	Properties of Al alloy: thermal conductivity	W/m/K	168
14	$\{\rho_{\text{w}}, \rho_{\text{c}}, \rho_{\text{e}}, \rho_{\text{p}}\}$	Properties of Al alloy: density	kg/m^3	2700
15	y_{w}	Maximal allowable deflection in the saddle	m	10^{-4}
16	n_{g}	Acceleration level for ground mechanical test	–	14

The assembly parts and inner HP temperatures, fluid mass flow rates, pressure drops and hydraulic diameters compose the vector of regime parameters $\bar{y}_k = \{T_{\text{eq},k}, T_{\text{ep},k}, T_{\text{ev},k}, T_{\text{e},k}, T_{\text{ve},k}, T_{\text{vc},k}, T_{\text{c},k}, T_{\text{cp},k}, T_{\text{cw},k}, \varphi_k, \Delta P_{\text{l},k}, \Delta P_{\text{v},k}, \Delta P_{\text{lv},k}, \Delta P_{\text{g},k}, D_{\text{hp},k}, D_{\text{hv},k}, D_{\text{ha},k}, \dot{m}_{\text{l},k}, \dot{m}_{\text{la},k}\}$. Their values are calculated by a subroutine that encodes the HPRA mathematical model, and that is coupled to the optimization algorithm.

Finally, there are specific parameters associated to the phenomenon of liquid excess, whose magnitudes are defined by characteristics of the operational modes. They are the length of liquid slug at the end of the condenser at 0g, L_{p} and mass of HP fluid charge, M_{f}. Thus, the vector $\bar{y}_0$ has two components: $\bar{y}_0 = \{L_{\text{lp}}, M_{\text{f}}\}$. The calculation is performed by an iterative procedure internal to the HPRA model, denoted in the general statement of the optimization problem as $\bar{y}_0 = \Psi(\bar{x}, \bar{s}, \bar{y}_1, \bar{y}_2, \ldots, \bar{y}_k, \ldots, \bar{y}_N)$.

4. Objective function and constraints description

The objective function expresses the total mass of the assembly to be minimized:

$$\min_{\bar{x}} M_{\Sigma}(\bar{x}, \bar{s}, \bar{y}_0) = M_{\text{e}} + M_{\text{r}} + M_{\text{hp}} + M_{\text{f}}.$$

The components of the objective function are the masses of the saddle (M_{e}), radiator (M_{r}), heat pipe (M_{hp}) and fluid charge (M_{f}), respectively. In the model, these components are expressed straightforwardly through the basic geometric parameters, which compose a vector of optimized variables ($\bar{x}$).

Besides the objective function, there are a total of 48 constraints, $f_i(\bar{x}, \bar{s}, \bar{p}_k, \bar{r}_k, \bar{y}_k)$. These constraints are separated in six groups, one for each operational mode, plus the seventh group (functions $\varphi(\cdot)$), which unites all operational modes.

The first two constraints for each mode are derived from the design requirement that under all operational modes the equipment operational temperature must be kept within a defined range:

$T_{\min} \leqslant T_{\text{eq}} \leqslant T_{\max}$, or

$$f_1(\bar{x}, \bar{s}, \bar{p}_k, \bar{r}_k, \bar{y}_k) : \frac{T_{\text{eq},k}}{T_{\text{eq max},k}} \leqslant 1, \tag{1}$$

$$f_2(\bar{x}, \bar{s}, \bar{p}_k, \bar{r}_k, \bar{y}_k) : \frac{T_{\text{eq},k}}{T_{\text{eq min},k}} \geqslant 1. \tag{2}$$

The third constraint is derived from the required heat transfer capability:

$$f_3(\bar{x}, \bar{s}, \bar{p}_k, \bar{r}_k, \bar{y}_k) : \frac{Q_k}{Q_{x,k}} \geqslant 1. \tag{3}$$

It means that the calculated heat rate being transported under conditions of the kth operational mode, Q_k, should be equal or greater than the specified $Q_{x,k}$.

The next constraint is the HP capillary limit:

$$f_4(\bar{x},\bar{s},\bar{p}_k,\bar{r}_k,\bar{y}_k) : \frac{1}{\Delta P_{\mathrm{c}\max,k}}\left(\Delta P_{\mathrm{l},k}+\Delta P_{\mathrm{v},k}+\Delta P_{\mathrm{lv},k}+\Delta P_{\mathrm{g},k}\right) \leqslant 1. \tag{4}$$

The pressure drops are classified as regime parameters (i.e. components of the vector $\bar{y}_k$); their expressions are discussed in the next sections.

The remaining mode-dependent constraints (i.e. $f_5(\bar{x},\bar{s},\bar{p}_k,\bar{r}_k,\bar{y}_k)$ through $f_7(\bar{x},\bar{s},\bar{p}_k,\bar{r}_k,\bar{y}_k)$) are the boiling, sonic and entrainment limits, respectively. Commonly used expressions from Chi [8] were adopted here to build up these constraints.

The previous seven constraints are repeated for the six operational modes, making up a total of 42 effective constraints (functions $f(\cdot)$).

The mode-independent constraints R_x take into account different cases of mechanical loads over the HPRA. The stresses on the radiator plate and heat pipe are analyzed separately, using known plate and beam bending equations, and isostatic boundary conditions. The radiator is assumed to be a flat plate rigidly fixed to the HP wall (Fig. 2, case 2). The magnitude of the mechanical loads applied to the assembly is equivalent to the maximum acceleration expected at launch, although not considering its vibration modes and natural frequencies. Thus, only the bending effect from the inertia forces ($F_{\mathrm{c}} = M_{\mathrm{r}} n_{\mathrm{g}} g$) distributed over the radiator area ($B_{\mathrm{r}} L_{\mathrm{c}}$) is considered. The corresponding constraint is given by

$$\varphi_{43}(\bar{x},\bar{s}) : \frac{3\beta\rho_{\mathrm{c}} B_{\mathrm{r}}^2 n_{\mathrm{g}} g}{\delta_{\mathrm{r}} u_{\mathrm{c}}} \leqslant 1. \tag{5}$$

The tube is considered as rigidly attached to the condenser and saddle (Fig. 2, case 1), and the equivalent loads are derived from inertia forces. The radiator stiffness is neglected yielding a conservative evaluation. The maximum stress associated to the bending momentum applied on the tube is given by

$$\hat{\sigma}_{\mathrm{b}} = \frac{\hat{M}_{\max}(D_{\mathrm{v}} + 2\delta_{\mathrm{p}} + \delta_{\mathrm{w}})}{2I_{\mathrm{hp}}}, \tag{6}$$

where $\hat{M}_{\max}$ is defined from considering the balance of forces corresponding to loading case 2 in Fig. 2, and

$$I_{\mathrm{hp}} = \frac{\pi\left((D_{\mathrm{v}} + 2\delta_{\mathrm{p}} + 2\delta_{\mathrm{w}})^4 - (D_{\mathrm{v}} + 2\delta_{\mathrm{p}})^4\right)}{64}$$

The corresponding constraint is

$$\varphi_{44}(\bar{x},\bar{s}) : \frac{\beta\hat{\sigma}_{\mathrm{b}}}{u_{\mathrm{w}}} \leqslant 1. \tag{7}$$

The evaporator saddle is designed in order to limit deflection, in order to keep good thermal contact on the mechanical interface with the equipment. The saddle is assumed to be a beam of uniform thickness submitted to a central force F_{h} (Fig. 2, case 6). This force is derived from the maximum bending moment that may appear due to the action of equivalent inertia forces over the HP length

$$F_{\mathrm{h}} = \frac{\hat{M}_{\mathrm{s}}}{L_{\mathrm{e}}} = \frac{F_{\mathrm{a}} L_{\mathrm{a}} + F_{\mathrm{c}}(2L_{\mathrm{a}} + L_{\mathrm{c}}) + F_{\mathrm{p}}(2L_{\mathrm{a}} + 2L_{\mathrm{c}} + L_{\mathrm{p}})}{2L_{\mathrm{e}}}, \tag{8}$$

where $F_{\mathrm{a}} = (M_{\mathrm{hp}} + M_{\mathrm{f}}) n_{\mathrm{g}} g \frac{L_{\mathrm{a}}}{L}$; $F_{\mathrm{c}} = M_{\mathrm{r}} n_{\mathrm{g}} g$; $F_{\mathrm{p}} = (M_{\mathrm{hp}} + M_{\mathrm{f}}) n_{\mathrm{g}} g \frac{L_{\mathrm{a}}}{L}$.

The corresponding constraint is the limitation of deflection at the center of the saddle:

$$\varphi_{45}(\bar{x},\bar{s}) : \frac{F_{\mathrm{h}}(2B_{\mathrm{e}} + D_{\mathrm{v}} + 2\delta_{\mathrm{p}} + 2\delta_{\mathrm{w}})}{48 E I_{\mathrm{e}} y_{\mathrm{w}}} \leqslant 1, \tag{9}$$

where y_{w} is the maximal allowable deflection and $I_{\mathrm{e}} = \frac{L_{\mathrm{e}}\delta_{\mathrm{e}}^3}{12}$.

The thickness of the container wall and end caps must sustain the internal pressure (Fig. 2, case 5). The longitudinal and hoop stresses can be calculated by considering the heat pipe as a thin walled tube:

$$\hat{\sigma}_L = \frac{P_{\max}(D_{\mathrm{v}} + 2\delta_{\mathrm{p}} + \delta_{\mathrm{w}})}{4\delta_{\mathrm{w}}}, \quad \hat{\sigma}_\theta = \frac{P_{\max}(D_{\mathrm{v}} + 2\delta_{\mathrm{p}} + \delta_{\mathrm{w}})}{2\delta_{\mathrm{w}}}. \tag{10}$$

The associated constraint is

$$\varphi_{46}(\bar{x},\bar{s}) : \frac{\beta P_{\max}(D_{\mathrm{v}} + 2\delta_{\mathrm{p}} + \delta_{\mathrm{w}})}{2\delta_{\mathrm{w}} u_{\mathrm{w}}} \leqslant 1, \tag{11}$$

where $P_{\max}$ is the maximal design pressure.

One more condition is related to a possibility to hold the entire assembling by radiator edge during manipulations (Fig. 2, case 4). The bending moment is related to whole mass of the HPRA, assumed of eventual acceleration of $2g$. The associated constraint is

$$\varphi_{47}(\bar{x},\bar{s}) : \frac{12 g M_{\Sigma}(0.5D_{\mathrm{v}} + \delta_{\mathrm{p}} + \delta_{\mathrm{w}} + B_{\mathrm{r}})\delta_{\mathrm{r}}}{\delta_{\mathrm{r}}^3 L_{\mathrm{c}} u_{\mathrm{c}}} \leqslant 1. \tag{12}$$

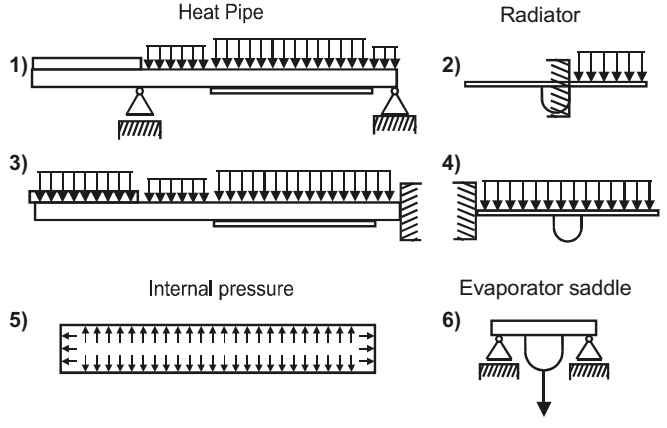

Fig. 2. Mechanical loading cases.

Another condition is a possibility of holding the entire assembly by the condenser end during hand manipulations (Fig. 2, case 3). The maximum bending moment is

$$\hat{M}_{\mathrm{hdl}} = 2g\big((M_{\mathrm{e}} + M_{\mathrm{f}})(0.5L_{\mathrm{e}} + L_{\mathrm{a}} + L_{\mathrm{c}} + L_{\mathrm{p}}) + 0.5M_{\mathrm{hp}}L + M_{\mathrm{r}}(0.5L_{\mathrm{c}} + L_{\mathrm{p}})\big). \quad (13)$$

The associated bending stress is therefore

$$\hat{\sigma}_{\mathrm{b}} = \frac{\hat{M}_{\mathrm{hdl}}(D_{\mathrm{v}} + 2\delta_{\mathrm{p}} + \delta_{\mathrm{w}})}{2I_{\mathrm{hp}}},$$

$$I_{\mathrm{hp}} = \frac{\pi\Big((D_{\mathrm{v}} + 2\delta_{\mathrm{p}} + 2\delta_{\mathrm{w}})^4 - (D_{\mathrm{v}} + 2(1-\varepsilon)\delta_{\mathrm{p}})^4\Big)}{64}, \quad (14)$$

where $\varepsilon = \frac{w}{w+b}$. The resultant constraint is

$$\varphi_{48}(\bar{x}, \bar{s}) : \frac{\hat{\sigma}_{\mathrm{b}}}{u_{\mathrm{w}}} \leqslant 1. \quad (15)$$

Thus, the optimization problem is composed by 48 constraints bonding up to six operational modes. The developed algorithm has a feature to switch-off some operational modes, if necessary.

5. Mathematical model of HP radiator assembly

The key dimensions of the assembly as well as the HP groove parameters are shown in Fig. 1. At 0g conditions, the radiator reject heat to space and is exposed to external incident fluxes. At ground thermal vacuum test conditions, the radiator emits heat to the vacuum chamber internal shroud.

The HPRA model presented in this section is a system of algebraic equations, denoted by $\{\Phi, \tilde{\Phi}, \Psi\}$ in the general statement of the optimization problem. The model consists of hydraulic and thermal parts.

5.1. Hydraulic part

In the HP under 0g conditions, the pressure balance along the fluid path is expressed as

$$\Delta P_{\mathrm{c\,max}} \geqslant \Delta P_{\mathrm{l}} + \Delta P_{\mathrm{v}} + \Delta P_{\mathrm{lv}} + \Delta P_{\mathrm{g}}. \quad (16)$$

The pressure drop for liquid flow through the wick structure is based on Darcy's law

$$\Delta P_{\mathrm{l}} = \frac{\mu_{\mathrm{l}}(T_{\mathrm{e}})\dot{m}_{\mathrm{l}}}{2A_{\mathrm{l}}\rho_{\mathrm{l}}\varepsilon K}L_{\mathrm{e}} + \frac{\mu_{\mathrm{l}}(T_{\mathrm{a}})\dot{m}_{\mathrm{l}}}{A_{\mathrm{l}}\rho_{\mathrm{l}}\varepsilon K}L_{\mathrm{a}} + \frac{\mu_{\mathrm{l}}(T_{\mathrm{c}})\dot{m}_{\mathrm{l}}}{2A_{\mathrm{l}}\rho_{\mathrm{l}}\varepsilon K}L_{\mathrm{c}}, \quad (17)$$

where

$$K = \frac{D_{\mathrm{hp}}^2}{2(fRe)_{\mathrm{l}}}, \quad D_{\mathrm{hp}} = \frac{4\delta_{\mathrm{p}}w}{2\delta_{\mathrm{p}} + w}, \quad a = \frac{w}{\delta_{\mathrm{p}}}, \quad \varepsilon = \frac{w}{w+b}.$$

For rectangular channels, Shah and Bhatti [13] found that

$$(fRe)_{\mathrm{l}} = 24(1 - 1.3553a + 1.9467a^2 - 1.7012a^3 + 0.9564a^4 - 0.2537a^5). \quad (18)$$

It holds 0.05% error if $0 < a < 1$. Following Faghri [7] this equation is applicable to the configuration of the grooves shown in Fig. 1. Faghri and Parvani [14] have developed an analytical model for the pressure lost in the vapor channel under the assumption of incompressible flow,

$$\Delta P_{\mathrm{v}} = \Delta P_{\mathrm{ve}} + \Delta P_{\mathrm{va}} + \Delta P_{\mathrm{vc}} = \left(\frac{1}{2} + \frac{1}{3}Re_{\mathrm{e}}\right)\frac{128\mu_{\mathrm{v}}\dot{m}_{\mathrm{v}}}{\pi\rho_{\mathrm{v}}D_{\mathrm{v}}^4}L_{\mathrm{e}} + \frac{128\mu_{\mathrm{v}}\dot{m}_{\mathrm{v}}}{\pi\rho_{\mathrm{v}}D_{\mathrm{v}}^4}L_{\mathrm{a}} + \left(\frac{1}{2} - \frac{1}{3}Re_{\mathrm{e}}\right)\frac{128\mu_{\mathrm{v}}\dot{m}_{\mathrm{v}}}{\pi\rho_{\mathrm{v}}D_{\mathrm{v}}^4}L_{\mathrm{c}}. \quad (19)$$

The liquid–vapor frictional interaction is described by the model, given by Schneider and DeVos [15], and recommended by Faghri [7] for rectangular grooves,

$$\Delta P_{\mathrm{lv}} = \frac{\mu_{\mathrm{l}}\dot{m}_{\mathrm{l}}\psi}{A\rho_{\mathrm{l}}\varepsilon K}L_{\mathrm{eff}}, \quad (20)$$

where $\psi = \frac{w^3}{6(w+b)D_{\mathrm{v}}^2}\cdot(fRe)_{\mathrm{v}}\frac{\mu_{\mathrm{v}}\rho_{\mathrm{l}}}{\mu_{\mathrm{l}}\rho_{\mathrm{v}}}\left[1 - 1.971\cdot\exp\left(-\frac{\pi\delta_{\mathrm{p}}}{w}\right)\right]$.

The possible pressure drop due to small accelerations caused by actions of the attitude control sub-system can be estimated, in a conservative approach, by

$$\Delta P_{ng} = \max\left(\ddot{\omega}, \frac{\dot{\omega}^2}{2}\right)\rho_{\mathrm{l}}L^2. \quad (21)$$

Here $\ddot{\omega}, \dot{\omega}$ are the angular acceleration of the satellite and radial velocity correspondingly. Dependent on the satellite control system conception, these values could be either negligible (if only reaction wheels are used) or significant (if thrusters are used).

At 1g conditions, the body-force term in the pressure balance along the HP fluid path changes to

$$\Delta P_{\mathrm{g}} = \rho_{\mathrm{l}}g\delta_{\mathrm{t}}. \quad (22)$$

Besides that, the expression for the capillary pressure is modified to include the conditions for maintaining the liquid in upper grooves:

$$\Delta P_{\mathrm{c\,max}} = \frac{2\sigma'\cos\theta_{\min}}{w} - \rho_{\mathrm{l}}g(\delta_{\mathrm{p}} + \delta_{\mathrm{t}}). \quad (23)$$

Under ground conditions, if the HP is positioned horizontally, the excess of liquid usually develops a puddle at the bottom of the vapor channel, if $Bo > 1$. This puddle affects the behavior of the HP by several ways [22]. Here we consider the following: first, the puddle behaves as an eventual artery providing reduced hydraulic resistance for liquid return; second, the thermal resistance for heat transfer in radial direction increases; and third, the vapor channel becomes narrower causing increasing hydraulic losses in vapor space.

The liquid flow is divided in two parallel paths: through the HP grooves and through the eventual artery,

$$\dot{m}_{\mathrm{l}} = \dot{m}_{\mathrm{lw}} + \dot{m}_{\mathrm{ar}}. \quad (24)$$

The hydraulic diameter of the artery is

$$D_{\mathrm{har}} \cong \frac{D_{\mathrm{v}}\big(\varphi(1 + \varepsilon\delta_{\mathrm{p}}) - \sin\varphi\big)}{\varphi\Big(1 + \varepsilon + \frac{2\delta_{\mathrm{p}}}{(w+b)}\Big) + 2\sin\frac{\varphi}{2}}. \quad (25)$$

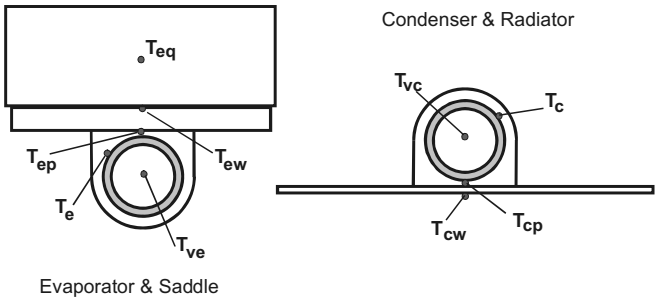

Fig. 3. Temperatures definition.

It is assumed that the liquid–vapor frictional interaction occurs only over the grooves and not over the puddle artery, because the velocity of the liquid inside the artery is lower than velocity inside the grooves.

5.2. Thermal part

At $0g$ the heat balance at steady state for the heat transfer from attached equipment to the HP evaporator saddle is defined as

$$Q = g_{eq} L_e \left(2\eta_e B_e + D_v + 2\delta_p + 2\delta_w\right)(T_{eq} - T_{ew}), \tag{26}$$

where g_{eq} is the overall thermal conductance from the equipment, (or a thermal–mechanical interface) to the saddle surface, including the thermal contact resistance. The positions of the reference temperatures are shown in Fig. 3.

It is assumed that over the saddle surface, where the HP is attached, the temperature does not change, only along its fin. The thermal effectiveness of the saddle fin is given by

$$\eta_e = \frac{\tanh(mB_e)}{mB_e}; \quad m = \sqrt{\frac{g_{eq}}{k_e \delta_e}}.$$

The heat transfer between the saddle and the HP external surface, through the HP wall, and from the HP internal surface to the evaporator core is defined by the following balance equations, respectively,

$$\begin{aligned} Q &= (T_{ew} - T_{ep})\frac{k_e}{\delta_e} L_e (D_v + 2\delta_p + 2\delta_w + 2B_e\eta_e), \\ Q &= (T_{ep} - T_e)\frac{k_w}{\delta_w} L_e \left(\pi(D_v + 2\delta_p)\eta_w\right), \\ Q &= (T_e - T_{ve})\frac{k_{pe}}{\delta_p}\pi L_e D_v, \end{aligned} \tag{27}$$

where η_w is the thermal effectiveness of the tube wall, which is considered as a one-dimensional conducting fin. The same approach is referred in [23]:

$$\eta_w = \frac{\tanh(pD_v\varsigma)}{pD_v\varsigma}; \quad p = \sqrt{\frac{k_p}{k_w\delta_w\delta_p}}; \quad \varsigma = \frac{\pi}{2} + \frac{\delta_p}{D_v}. \tag{28}$$

The effective thermal conductivity, k_{pe}, is defined by the relationship derived for the evaporation from rectangular grooves by Chi [8].

The heat balance between the radiator and the space environment in flight conditions ($0g$) is given by

$$Q = (\varepsilon_r\sigma_r T_{cw}^4 - q_{ext})L_c\left(2\eta_r B_r + D_v + 2(\delta_w + \delta_p)\right), \tag{29}$$

where q_{ext} is the absorbed external heat flux,

$$q_{ext} = \alpha_r(q_s + q_A) + \varepsilon_r q_{IR}. \tag{30}$$

The thermal effectiveness of the radiator is given by

$$\eta_r = \frac{\tanh(rB_r)}{rB_r}; \quad r = \sqrt{\frac{4\varepsilon_r\sigma_r T_{cw}^3}{k_r\delta_r}}. \tag{31}$$

At the condenser side, the balance of energy is similar to the evaporator side.

At $1g$ conditions, the radiator heat balance for the thermal vacuum test is determined by a different relationship in respect to $0g$ conditions:

$$Q = \sigma_r\varepsilon_r\varepsilon_{rvc}(T_{cw}^4 - T_{rvc}^4)L_c\left(2\eta_r B_r + D_v + 2(\delta_w + \delta_p)\right). \tag{32}$$

The vapor temperature in the condenser core, T_{ce}, is related to vapor evaporator temperature, T_{ve}, through the Clausius–Clapeyron equation. The overall heat and mass balances link the hydraulic and heat parts of the model:

$$Q = \lambda(T_{vc})\cdot\dot{m}_l; \quad \dot{m}_l = -\dot{m}_v. \tag{33}$$

The HPRA model is solved numerically by a sequence of calculations with several iteration loops. The parameters $\{T_{ve,k}, T_{cw,k}, \varphi_k\}$ are calculated by internal loops for each kth operational mode, and parameters $\{L_{lp}, M_f\}$ are calculated by an external loop. The other parameters are calculated by consequent substitution.

6. Validation of the model

The numerical model used in this work has been validated by comparison with published experimental results of ground performance tests of a grooved aluminum HP,

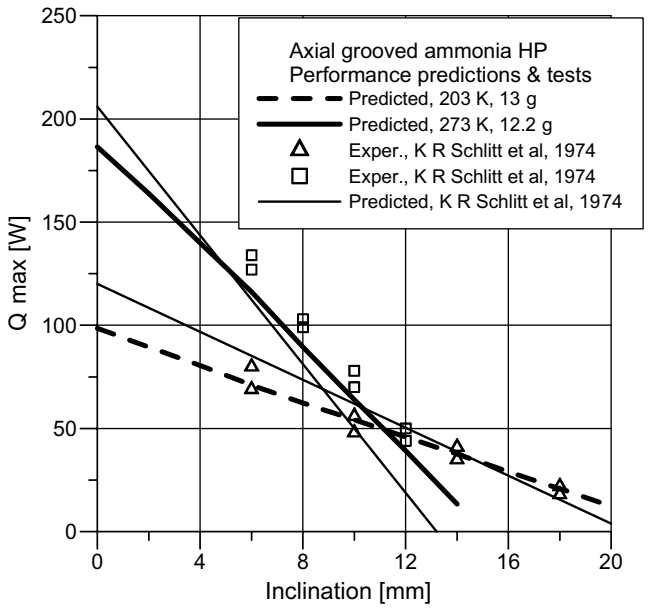

Fig. 4. The HP model verification.

published by Schlitt [9]. To perform this comparison, the model was re-arranged in such a way that all geometric parameters were fixed to the values presented in that paper, as well as the mass of fluid charge and HP tilt. The strength constrains for this comparison were deactivated. Neither the saddle nor the radiator was considered, following the described test setup.

Experimental and numerical results are shown in Fig. 4 for two cases with different average work temperature (203 K and 273 K) and fluid charge (13g and 12.2g). As can seen, the numerical results fit well the experimental data.

7. The GEO algorithm

The generalized extremal optimization algorithm is a new global search meta-heuristic developed to be applied to complex optimization problems. It is based on the extremal optimization (EO) method proposed by Boettcher and Percus [16], that was inspired by the simplified evolutionary model of Bak and Sneppen [17]. Belonging to the general class of stochastic methods, GEO can be turned to a deterministic pure random search through its only adjustable parameter. It can deal with any kind of design variable either continues, integer, discrete or a combination of them. Not depending on derivatives of the objective function or constraints, it can be applied to highly nonlinear problems, that presents a multimodal, or even disjoint, design space. In GEO a string of bits encodes the design variables. Being an evolutionary algorithm, each bit is considered a species and has an associated fitness. This number depends on the adaptability of the bit, that in GEO is related to the improvement or not on the value of the objective function

Table 3
Results of optimization

Input			Output	$\bar{x}$ [mm]											$\bar{y}_0$	
Fluid	Modes	Q_x [W]	Mass [kg]	D_v	L_e	L_c	B_e	B_r	δ_e	δ_r	δ_w	δ_p	w	b_w	L_p [mm]	M_f [g]
			$\mathbf{x}^-$:	1...	10...	10...	10...	10...	0.4...	0.12	0.4...	0.2...	0.01	0.4...		
			$\mathbf{x}^+$:	103	1014	1014	191	400	50	12.5	10	20	2	4.9		
Amm	1	20	0.085	4.1	184.7	782.0	5.0	45.0	2.1	0.15	0.69	0.54	0.54	0.40	0.0	3.6
Amm	1	40	0.376	8.4	321.2	621.4	5.2	131.0	2.9	0.49	1.08	0.64	0.64	0.40	0.0	9.4
Amm	1	60	0.729	11.0	550.2	1253.4	5.0	80.0	3.8	0.46	1.31	1.38	1.36	0.40	0.0	55.6
Amm1	80	1.347	13.8	553.8	1168.6	5.0	143.8	5.5	0.60	2.20	1.38	1.22	0.40	0.0	64.9	
Amm	1, 3	20	0.115	6.1	121.0	633.0	5.3	67.2	2.4	0.12	1.36	0.47	0.47	0.40	5.8	4.0
Amm	1, 3	40	0.388	8.5	325.6	711.8	5.0	110.1	2.9	0.46	1.08	0.95	0.95	0.40	15.4	18.4
Amm	1, 3	60	0.801	10.5	339.8	1089.2	5.0	120.9	5.5	0.46	2.20	0.95	0.94	0.42	15.5	28.2
Amm*	1, 3	80	1.362	17.8	398.9	976.8	5.1	154.7	5.5	0.83	1.98	0.95	0.95	0.40	3.1	44.1
Amm	1, 3, 5	20	0.115	6.1	121.0	633.0	5.3	67.2	2.4	0.12	1.36	0.47	0.47	0.40	5.3	3.9
Amm	1, 3, 5	40	0.389	8.6	324.5	702.0	5.0	112.5	2.9	0.46	1.08	0.95	0.95	0.40	15.0	18.4
Amm	1, 3, 5	60	0.800	12.8	328.9	936.5	5.0	121.9	5.5	0.64	1.41	0.95	0.95	0.40	8.8	31.2
Amm	1, 3, 5	80	1.296	19.1	466.2	1099.6	5.7	132.5	5.5	0.56	2.20	0.95	0.94	0.41	7.6	53.7
Acet	1	20	0.122	6.3	83.0	879.7	5.9	43.4	3.8	0.10	0.41	1.48	1.48	0.40	0.0	29.6
Acet	1	40	0.308	7.1	195.9	1156.4	7.3	62.4	5.0	0.22	0.48	1.87	1.49	0.42	0.0	50.2
Acet	1	60	0.571	12.6	321.8	1176.5	5.8	99.5	6.0	0.31	0.56	1.40	1.38	0.42	0.0	68.8
Acet	1	80	0.927	13.3	346.1	1195.4	12.7	133.4	5.7	0.48	0.57	1.63	1.50	0.40	0.0	89.8
Acet	1, 3	20	0.142	6.7	147.8	462.7	5.7	80.0	2.5	0.31	0.42	1.23	1.22	0.40	0.6	18.0
Acet	1, 3	40	0.351	9.4	320.7	740.5	6.3	108.3	2.9	0.29	0.40	1.86	1.50	0.40	18.4	60.9
Acet	1, 3	60	0.642	18.1	268.2	1093.5	10.1	93.8	5.5	0.38	0.40	1.34	1.34	0.40	10.6	89.1
Acet*	1, 3	80	0.965	19.0	407.7	1197.9	6.0	123.8	5.5	0.51	0.40	1.50	1.49	0.40	12.9	122.4
Acet	1, 3, 5	20	0.157	8.4	82.7	455.3	5.4	100.0	5.5	0.30	0.40	0.95	0.88	0.40	10.7	14.6
Acet	1, 3, 5	40	0.405	19.5	86.0	886.4	6.0	103.8	7.3	0.31	0.40	1.00	0.88	0.40	9.8	50.0
Acet	1, 3, 5	60	0.914	19.3	180.3	975.6	7.0	120.8	9.0	0.55	0.45	1.85	0.67	0.40	11.2	97.3
Acet	1, 3, 5	80	1.582	66.9	110.0	1153.3	21.3	93.5	16.0	0.46	0.40	0.95	0.81	0.40	2.9	182.9
$L_e < 300$ mm and $L_c < 800$ mm																
Amm*	1, 3	80	2.044	20.3	300.0	800.0	22.9	200.6	9.2	1.03	2.45	0.86	0.48	1.41	3.8	16.4
Acet*	1, 3	80	1.551	39.1	299.9	799.9	13.6	183.9	7.5	0.86	0.40	1.06	1.06	0.40	2.8	116.7
$\beta = 2.5$																
Amm*	1, 3	80	1.025	19.1	326.2	1257	5.16	123.7	6.38	0.48	1.3	0.98	0.95	0.4	3.34	56.28
Acet*	1, 3	80	0.965	19.0	407.7	1197.9	6.0	123.8	5.5	0.51	0.40	1.50	1.49	0.40	12.9	122.4
$L_e < 300$ mm, $L_c < 800$ mm and $\beta = 2.5$																
Amm*	1, 3	80	1.598	21.7	300	800	11.5	225.5	7.34	0.94	1.45	0.64	0.53	0.64	5.83	22.84
Acet*	1, 3	80	1.494	36.2	300	799.9	5.10	220.6	7.29	0.83	0.41	0.97	0.89	0.44	2.62	90.84
$L_e < 300$ mm, $L_c < 800$ mm, $\beta = 2.5$, $h_e = 4.8 * h_e$ and $h_c = 0.21 * h_c$																
Amm*	1, 3	80	1.536	16.3	299.9	800	17.5	231.3	7.25	0.97	1.05	0.72	0.72	0.44	0.49	23.6
Acet*	1, 3	80	1.455	36.1	299.9	799.9	5.0	220.3	6.82	0.83	0.4	0.97	0.97	0.41	2.84	95.75

if the bit is flipped. GEO has been applied successfully to real complex design problems, including HP design [3,4]. It also has proved to be competitive to other popular stochastic algorithms such as genetic algorithm and simulating annealing [18], with the a priori advantage of having only one free parameter to tune. A detailed description of the algorithm can be found in [18,19].

8. Results

The optimization was performed considering either operational mode 1, 1 and 3 or 1, 3 and 5. The last corresponds fixed specified heat load $Q_{\max}$ considered for "hot" (mode 1) and "cold" (mode 3) conditions over the radiator, and one mode for ground test conditions (mode 5). The boundary limits for the equipment temperature was established as $[-10, +45\ ^{\circ}\mathrm{C}]$. Heat loads $Q_{x,k} = Q_{\max}$, applied on the evaporator, varied 20, 40, 60 and 80 W. At condition of ground test the temperature of the shroud of vacuum chamber was set to $-170\ ^{\circ}\mathrm{C}$ and a reduced heat load was accepted, namely $Q_{\mathrm{tst5}} = 0.75 * Q_{\max}$. The best results are given in Table 3.

It is interesting to note that the optimal values of almost all design variables, except b_{w}, do not reach its bound limits. It confirms the correctness of the optimization problem statement: all physical phenomena were modeled appropriately and the optimal design dimensions found did not reach the constraints boundaries (x_i^-, x_i^+). In the case of b, the limiting factor is the technological difficulty to fabricate an extrusion die with such a small opening.

In Fig. 5 the best 300 solutions found during the global minimum searching are shown as a function of the diameter of the vapor core, D_{v}. The figure displays the case for $Q = 60$ W, mode 1, with acetone. The other cases had approximately a similar distribution of points. From Fig. 5 it can be seen that the optimal point is located well within the dimensional limits of D_{v}. The density of shoots near the optimum is relatively low: the difference between optimal and nearest (sub-optimal) points is about 2%, which can be accepted as evaluation of achieved precision. The refining of solution can be easily achieved by additional run of the optimization problem with narrowed boundaries.

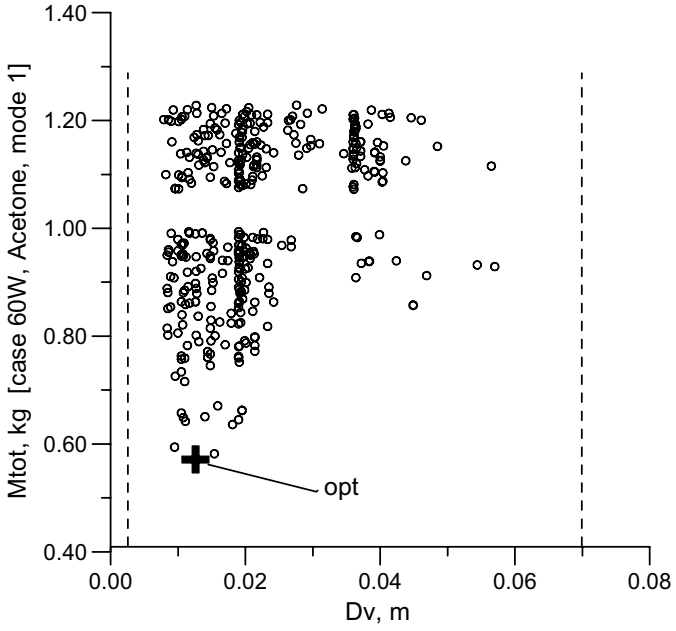

Fig. 5. Best 300 results of seeking by GEO and GEOvar.

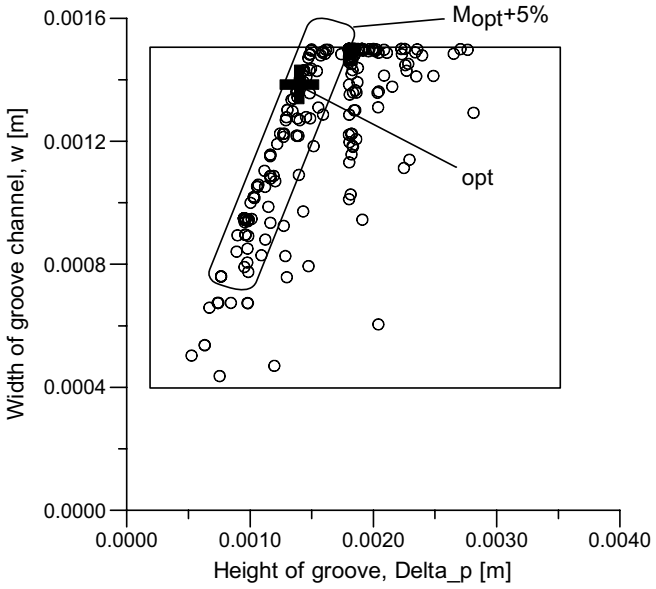

Fig. 6. Near-optimal solutions in variables' cut-plane.

The graph in Fig. 6 depicts the best 300 values found for the design variables w and δ_{p}. The domain of non-feasible combinations of variables may be evidently detected in the left-upper area of the graph. The zone of near-optimal solutions (optimum + 5%) forms an apparent ravine with a steep slope to the left and a smooth slope to the right. This gives a good notion about the behavior of the objective function in the selected cut-plane of the design space.

Optimal geometries for the assemblies, obtained by the present study, are summarized in Fig. 7. It is remarkable

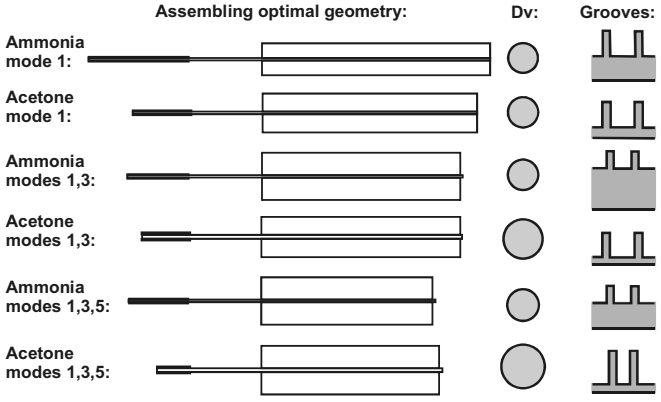

Fig. 7. Optimal configurations of the assembling for the heat loads of 60 W and for safety factor $\beta = 4$.

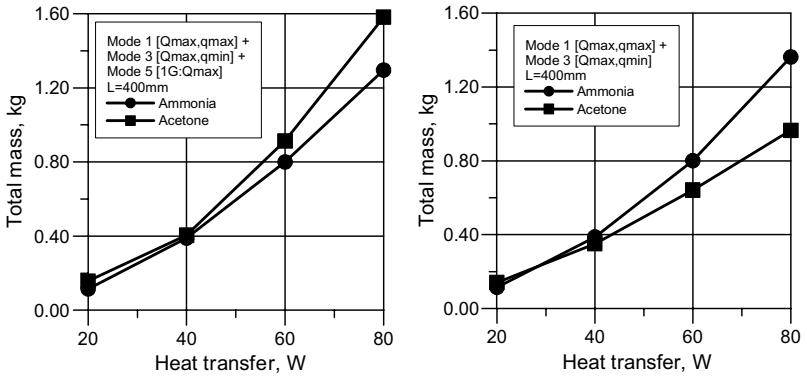

Fig. 8. Optimal HPRA mass characteristics for three and two modes, and for safety factor $\beta = 4$.

that all optimal configurations have a long-length radiator and long-length evaporator saddle. The optimal values of the radiator form factor, B_r/L_c lay within the range of about 0.05–0.15. In general, some real restrictions of satellite layout and equipment interfaces areas may limit some dimensions. Nevertheless, it is important for the designer engineer to know about the optimal geometries and minimal reachable values of assembly mass. Any divergence from the optimal geometry may cause a mass penalty for the HPRA, that can be re-calculated by introducing the additional constraints.

As an example, two cases with two supplementary constraints to the length of saddle ($L_e < 300$ mm) and condenser ($L_c < 800$ mm) have been run for the maximal heat load. The results show that such an adaptation to real project and corresponding deviation from the optimal geometry "costs" about from 50% to 61% of mass increasing for both assemblies. Remain optimal dimensions are changed to compensate such implementation of the additional constraints, as it may be seen from Table 3 (the lines are marked by asterisks). The left graph in Fig. 8 shows the optimal mass characteristics of two HPRA designed for ammonia and acetone, considering three operational modes, 1, 3 and 5. The total mass values differ no more than 18%, with the ammonia HPR assembly having the best mass characteristics. The fifth mode is a mode of ground testing, and if this 1*g* mode were not considered and only 0*g* modes were accounted (i.e. 1 and 3), the result is remarkably opposite: the acetone HP presents better mass characteristics by about 29% (Fig. 8, graph on the right).

Another parameter to be evaluated, is the chosen value for the safety factor. A magnitude of 4.0 may be too much conservative for well-developed technology of ammonia HP. In the NASA safety requirements [24], the factor 2.5 is recommended for HPs, keeping 4.0 for other unspecific pressurized components, which include also recent HP-like technologies, LHP, for example [25]. To see sensitivity to this parameter, the optimization was repeated assuming $\beta = 2.5$ for 80 W heat load under 1 and 3 modes. The results, given in Table 3, show a decreasing of the ammonia assembly mass around 25%, since the lower safety factor makes possible to reduce wall thickness of the high-pressure ammonia HP. The optimal configuration of acetone HP assembly stays unchangeable.

If both β is reduced to 2.5 and additional constraints to the lengths are applied, the acetone HP assembly wins the trade by only 7%.

In the present model the equivalent heat transfer coefficients vary within the ranges $h_e = 1300$–1600 and $h_c = 62{,}000$–$70{,}000$ W/m^2/K. However for ammonia HP the experiments reveal $h_e \approx 7000$ and $h_c \approx 13{,}600$ W/m^2/K [9,23]. To evaluate the effect of this uncertainty in optimal parameters, the corresponding factors 4.8 and 0.21 have been introduced in the model to take into account the experimental data; then additional runs have been performed. Results, also placed in Table 3, show an improvement of mass characteristics from 3% to 4% for all designs, keeping comparative trends unchangeable.

Finally, all results from Table 3 have been checked out for *Bo* number. The values vary as following: for ammonia $Bo = 1.05$–26.7 and for acetone 3.4–34.5. It confirms the accepted preposition that slug does not form at 1*g* conditions. However, for the heat load lesser than 20 W, when optimal HP diameter becomes smaller, the excess liquid configuration at 1*g* may switch to slug for ammonia HP.

9. Conclusion

In this paper the optimal characteristics of a heat pipe assembly for a space application were analyzed. The assembly consisted of a grooved type heat pipe coupled to a radiator plate and a saddle. The design variables comprised all dimensions of the assembly. The optimization was performed for different operational modes considered simultaneously, in 1*g* and 0*g*. As far as we know, this approach has never been done before. Puddle and slug formations due to excess of liquid were accounted. Mechanical strength constraints were also included in the problem. Two working fluids were considered.

For the optimization, the generalized extremal optimization method was used. It is a recently developed stochastic algorithm, that has been applied effectively to complex optimal design problems.

Results show that for the operational modes at 1*g* and 0*g* the best HP design found for acetone had a poorer mass characteristic compared to HP designed with ammonia (the difference is up to 18% in the ammonia favor). On the other hand, if only the 0*g* modes were taken into account, the assembly with acetone HP can be much more weight effective than the one with ammonia (from 7% up to 29% in the acetone favor, depends of input parameters). It is interesting to note, that the liquid transport factor criterion indicates an opposite trend: the LTF for ammonia is higher than for acetone by 3.34–5.47 times (from +45 °C to −20 °C).

The results also show that an adaptation to real project and corresponding deviation from the optimal geometry may "cost" from 50% to 61% of mass increasing for both assemblies, depending of input parameters for given restrictions on lengths.

This result indicates clearly that using acetone in this kind of HP assembly is a good alternative for the use of hazardous high-pressure ammonia when designing it for only 0*g* conditions. Note that the optimal design parameters for each working fluid are different. Because having a lighter device in orbit is the goal for a space application, the requirement for ground testing should not be the design driver. Hence, one should provide special suitable conditions for ground testing of such HP.

References

[1] W.B. Bienert, E.A. Skrabek, Heat Pipe Design Handbook, Dynatherm Corp., Report to NASA, NASA-CR-134264, Contract No. NAS9-11927, 1972, pp. D31–D40.

[2] R. Schlitt, Performance characteristics of recently developed high-performance heat pipes, Heat Transfer Eng. 16 (1) (1995) 44–52.

[3] V.G. Rajesh, K.P. Ravindran, Optimum heat pipe design: a nonlinear programming approach, Int. Commu. Heat Mass Transfer 24 (3) (1977) 371–380.

[4] F.L. Sousa, V.V. Vlassov, F.M. Ramos, Heat pipe design through generalized extremal optimization, Heat Transfer Eng. 25 (7) (2004) 34–45.

[5] J.-M. Tournier, M.S. El-Genk, A heat pipe transient analysis model, Int. J. Heat Mass Transfer 37 (5) (1994) 753–762.

[6] A. Mikheyev, N. Loginov, D. Michurin, Mathematical model and experimental investigation of transient behavior of heat pipe, in: Yu. Maidanic (Ed.), Heat Pipes: Science Technology Application, Proceeding of 12th International Heat Pipes Conference, Institute of Thermal Physics, Russia, 2002, pp. 494–502.

[7] A. Faghri, Heat Pipe Science and Technology, Taylor & Francis, 1995, pp. 61–264.

[8] W. Chi, Heat Pipe Theory and Practice, A Sourcebook, Hemisphere Publishing Corporation, 1976, pp. 33–95.

[9] K.R. Schlitt, P.J. Brennan, J.P. Kirkpatrick, Parametric performance of extruded axial grooved heat pipes from 100 to 300 K, in: Progress in Astronautics and Aeronautics: Heat Transfer with thermal Control Applications, vol. 39, 1975, pp. 215–227.

[10] F.L. Sousa, V. Vlassov, F.M. Ramos, Generalized extremal optimization: an application in heat pipe design, Appl. Math. Modell. 28 (2004) 911–931.

[11] G.P. Peterson, An Introduction to Heat Pipes: Modeling, Testing, and Applications, John Wiley & Sons, Inc., 1994, pp. 44–159.

[12] N.B. Vargaftik, Y.K. Vinogradov, V.S. Yargin, Handbook of Physical Properties of Liquids and Gases, third ed., Begell House, Inc., NY, Wallingford (UK), 1996, pp. 747–853.

[13] R.K. Shah, M.S. Bhatti, Laminar convective heat transfer in ducts, in: S. Kakai, R.K. Shah, W. Aung (Eds.), Handbook of Single-Phase Convective Heat Transfer, Wiley, New York, 1987, pp. 31–137, Chapter 3.

[14] A. Faghri, S. Parvani, Numerical analysis of laminar flow in a double-walled annular heat pipe, AIAA J. Thermophys. Heat Transfer 2 (3) (1987) 165–171.

[15] G.E. Schneider, R. DeVoz, Nondimensional analysis for the heat transport capability of axially-grooved heat pipes including liquid/vapor interaction, in: 18th Aerospace Sciences Meeting, AIAA Paper No. 1980-0214, Pasadena, CA, January 14–16, 1980, pp. 1–10.

[16] S. Boettcher, A.G. Percus, Optimization with extremal dynamics, Phys. Rev. Lett. 86 (2001) 5211–5214.

[17] P. Bak, K. Sneppen, Punctuated equilibrium and criticality in a simple model of evolution, Phys. Rev. Lett. 71 (24) (1993) 4083–4086.

[18] F.L. Sousa, F.M. Ramos, P. Paglione, R.M. Girardi, New stochastic algorithm for design optimization, AIAA J. 41 (9) (2003) 1808–1818.

[19] F.L. Sousa, F.M. Ramos, R.L. Galski, I. Muraoka, Generalized extremal optimization: a new meta-heuristic inspired by a model of natural evolution, in: L.N. De Castro, F.J. Von Zuben (Eds.), Recent Developments in Biologically Inspired Computing, Idea Group Inc., 2004.

[20] W.H. Kelly, J.H. Reisenweber Jr., Optimization of a heat pipe radiator for spacecraft high-power TWTAs, in: IV International Heat Pipe Conference, The Royal Aeronautical society, London, September 7–10, 1981, pp. 1–12.

[21] J.E. Enninger, D.K. Edwards, Excess liquid in heat-pipe vapor spaces, in: L.S. Fletcher (Ed.), Heat Transfer and Thermal Control Systems, Progress in Astronautics and Aeronautics, vol. 60, AIAA, 1977, pp. 80–95.

[22] G.L. Fleishman, T.C. Chiang, R.D. Ruff, Oxygen heat pipe 0-G performance evaluation based on 1-G tests, Paper No. AIAA 91-1358-CP, Presented at the 26th AIAA Thermophysics Conference in Honolulu, Hawaii, June 24–26, 1991, pp. 9.

[23] Y. Kamotani, Effects of one-sided heat input and removal on axially grooved heat pipe performance, in: L.S. Fletcher (Ed.), Heat Transfer and Thermal Control Systems, Progress in Astronautics and Aeronautics, vol. 60, AIAA, 1977, pp. 23–38.

[24] Safety policy and requirements for payloads using the space transportation system, NSTS 1700.7B, 1989, p. 25, 58 pp.

[25] N. Dunbar, W. Supper, Spacecraft capillary pumped loop technology - towards a qualified thermal control tool, in: 10th International Heat Pipe Conference, September 21–25, Stuttgart, Germany, 1997, pp. 1–6.